Electronic structure and interfacial properties of BeTe/Si, BeTe/Ge, and BeTe/SiGe superlattices

1997 J. Phys.: Condens. Matter 9 8055

(http://iopscience.iop.org/0953-8984/9/38/011)

J. Phys.: Condens. Matter **9** (1997) 8055–8064. Printed in the UK PII: S0953-8984(97)83401-7

Electronic structure and interfacial properties of BeTe/Si, BeTe/Ge, and BeTe/SiGe superlattices

Liqiang Zhu and Liyuan Zhang

Department of Physics, Peking University, Beijing 100871, People's Republic of China

Received 14 April 1997, in final form 16 June 1997

Abstract. An approach has been suggested for integrating the superior properties of the BeTe semiconductor with the mature technology of group IV semiconductors. In a semi-empirical sp^3s^* tight-binding scheme, detailed calculations of the electronic structures of the $(BeTe)_n/(Si_2)_m$, $(BeTe)_n/(Ge_2)_m$, and $(BeTe)_n/(SiGe)_m$ (110) superlattices are performed over a wide range of $n, m \leqslant 20$. It is found that the fundamental energy gap increases (up to 2.11 eV for BeTe/Si and 1.93 eV for BeTe/Ge at the $\tilde{X}$ point for $n = m = 2$) with decreasing superlattice period, and that the silicon or/and germanium layer plays an important role in determining the fundamental energy gap of the superlattice system due to the spatial quantum confinement effect. Two interface bands are identified in the upper region of the thermal gap in these systems, which extend over a quite different region of $\boldsymbol{k}$-space. Furthermore, the calculated electronic structure of $BeTe/Si_{1-x}Ge_{1+x}$ is found to be quite different from those of II–VI compounds grown on pure group IV semiconductors, but fairly close to their average.

1. Introduction

Semiconductor superlattices consisting of alternate layers of different materials provide extra dimensions for tailoring material properties. The combination of controlled variations in the composition, strain, and thickness of the layers provides electronic and optical properties [1–3] unlike those of any ordinary bulk material, that might lead to important applications in optoelectronics [4–7]. There has been great interest in the multilayer growth of II–VI compounds for optoelectronic device application in the visible-to-ultraviolet range, as strong nonlinearities in these materials and their quantum wells have been recognized for many years [8–10]. Of particular note for the present work is the successful fabrication of II–VI/IV superlattices using molecular beam epitaxy, with each layer consisting of a few monolayers of the constituent materials [11–13]. Since a detailed picture of the electronic structure and stability will provide guidance for device applications, the systematic study of the II–VI/IV superlattice systems has become a necessity from a practical point of view.

In this paper, we examine theoretically the electronic structures of BeTe/Si, BeTe/Ge, and BeTe/SiGe (110) superlattices by performing band-structure calculations using the tight-binding method. The (110) interface is nonpolar in a lattice-matched system, while the (100) and (111) interfaces are polar interfaces [14]. Therefore, the interface electric fields due to the differences of the nuclear charges between the two kinds of interface atom in a (100) or (111) growth direction will disappear in the present (110) growth case. Results for the charge densities of the confined states and interface states for these superlattice systems are also reported. A systematic study of the electronic and interfacial properties of II–VI/VI (110) superlattices with a wide range of epitaxial layer thickness has been carried out.

0953-8984/97/388055+10$19.50

2. The tight-binding technique

The tight-binding eigenstates of a superlattice can be expanded as a linear combination of atomic orbitals [14, 15]:

$$|\boldsymbol{k}, \lambda\rangle = \sum_{\xi,\alpha} \langle \xi, \boldsymbol{r}_\alpha, \boldsymbol{k}|\boldsymbol{k}, \lambda\rangle |\xi, \boldsymbol{r}_\alpha, \boldsymbol{k}\rangle = \sum_{\xi,\alpha} C_{\xi\alpha}(\boldsymbol{k}, \lambda)|\xi, \boldsymbol{r}_\alpha, \boldsymbol{k}\rangle \tag{1}$$

where λ denotes the band index, and ξ is a quantum number that runs over the basis orbitals s, s^*, p_x, p_y, and p_z at the different types of site α in a unit cell. The N wavevectors $\boldsymbol{k}$ lie in the first Brillouin zone with the origin of the lth unit cell at $\boldsymbol{R}_l$, and $\boldsymbol{r}_\alpha$ represents the positions of the atoms in this unit cell. $C_{\xi\alpha}(\boldsymbol{k}, \lambda)$ is the eigenwavefunction, which can be obtained by solving the Schrödinger equation:

$$\sum_{\xi',\alpha'} [\langle \xi, \boldsymbol{r}_\alpha, \boldsymbol{k}|\boldsymbol{H}|\xi', \boldsymbol{r}_{\alpha'}, \boldsymbol{k}\rangle - E_\lambda(\boldsymbol{k})\delta_{\xi\xi'}\delta_{\alpha\alpha'}]\langle \xi, \boldsymbol{r}_\alpha, \boldsymbol{k}|\boldsymbol{k}, \lambda\rangle = 0. \tag{2}$$

In this paper, only the nearest-neighbour interactions are included. Therefore, we obtain the following Hamiltonian matrix for $(\mathrm{II–VI})_n/(\mathrm{IV}_2)_m$ (110) superlattices:

$\langle \xi, \boldsymbol{r}_\alpha, \boldsymbol{k}|\boldsymbol{H}|\xi', \boldsymbol{r}_{\alpha'}, \boldsymbol{k}\rangle =$

$$\begin{bmatrix}
H_a & V_{ac} & 0 & U_{ac} & 0 & & & & & & & 0 & U_{Ca}^\dagger \\
 & H_c & U_{ca} & 0 & 0 & & & & & & & U_{Ac}^\dagger & 0 \\
 & & H_a & V_{ac} & 0 & U_{ac} & & & & & & & \\
 & & & H_c & U_{ca} & 0 & 0 & & & & & & \\
 & & & & & & \ddots & & & & & & \\
 & & & & & H_a & V_{ac} & 0 & U_{aC} & \ddots & & & \vdots \\
 & & & & & & H_c & U_{cA} & 0 & 0 & & & \\
 & & & & & & & H_b & V_{AC} & 0 & U_{AC} & & \\
 & & & & & & & & H_b & U_{CA} & 0 & 0 & \\
 & & \text{CC} & & & & & & & & \ddots & & 0 \\
 & & & & & & & & & & H_b & V_{AC} & 0 & U_{AC} \\
 & & & & & & & & & & & H_b & U_{CA} & 0 \\
 & & & & & & & & & & & & H_b & V_{AC} \\
 & & & & & & & & & & & & & H_b
\end{bmatrix} \tag{3}$$

where the total number of rows or columns of the Hamiltonian matrix is $n + m$, and each element represents a 5×5 matrix. The diagonal elements H_α (α = a, b, and c) correspond to intrasite energies, and the others contain the nearest-atomic interactions in the same layer ($V_{\alpha\alpha'}$) or between two neighbouring layers ($U_{\alpha\alpha'}$) perpendicular to the growth direction. The superlattice consists of two different semiconductors labelled a and c for a II–VI semiconductor compound and A and C for the group IV semiconductor silicon or germanium with a (110) interface. a and c are regarded as the anion and cation atoms of the II–VI group compound semiconductor, while for convenience A and C are used to distinguish two kinds of atom in silicon or germanium. b stands for the group IV

semiconductor silicon or germanium. Therefore, all elements in the Hamiltonian matrix are expressed as

$$H_{a(c)} = \begin{bmatrix} E_s^{a(c)} & 0 & 0 & 0 & 0 \\ & E_{s^*}^{a(c)} & 0 & 0 & 0 \\ & & E_p^{a(c)} & 0 & 0 \\ & & & E_p^{a(c)} & 0 \\ & & & & E_p^{a(c)} \end{bmatrix} \tag{4}$$

$$H_b = \begin{bmatrix} E_s^b & 0 & 0 & 0 & 0 \\ & E_{s^*}^b & 0 & 0 & 0 \\ & & E_p^b & 0 & 0 \\ & & & E_p^b & 0 \\ & & & & E_p^b \end{bmatrix} \tag{5}$$

$$V_{ac} = \begin{bmatrix} V_{(s,s)}P_1 & 0 & V_{(sa,pc)}P_2 & -V_{(sa,pc)}P_1 & 0 \\ 0 & 0 & V_{(s^*a,pc)}P_2 & -V_{(s^*a,pc)}P_1 & 0 \\ -V_{(sc,pa)}P_2 & -V_{(s^*c,pa)}P_2 & \mathrm{VP}_1 & -V_{(x,y)}P_2 & 0 \\ V_{(sc,pa)}P_1 & V_{(s^*c,pa)}P_1 & -V_{(x,y)}P_2 & V_{(x,x)}P_1 & 0 \\ 0 & 0 & 0 & 0 & [V_{(x,x)} - V_{(x,y)}]P_1 \end{bmatrix} \tag{6}$$

$$U_{ac} = \begin{bmatrix} V_{(s,s)}P_3 & 0 & 0 & V_{(sa,pc)}P_3 & V_{(sa,pc)}P_4 \\ 0 & 0 & 0 & V_{(s^*a,pc)}P_3 & V_{(s^*a,pc)}P_4 \\ 0 & 0 & \mathrm{VP}_3 & 0 & 0 \\ -V_{(sc,pa)}P_3 & -V_{(s^*c,pa)}P_3 & 0 & V_{(x,x)}P_3 & V_{(x,y)}P_4 \\ -V_{(sc,pa)}P_4 & -V_{(s^*c,pa)}P_4 & 0 & V_{(x,y)}P_4 & [V_{(x,x)} + V_{(x,y)}]P_3 \end{bmatrix} \tag{7}$$

$$U_{ca} = \begin{bmatrix} V_{(s,s)}P_5 & 0 & 0 & -V_{(sc,pa)}P_5 & V_{(sc,pa)}P_6 \\ 0 & 0 & 0 & -V_{(s^*c,pa)}P_5 & V_{(s^*c,pa)}P_6 \\ 0 & 0 & \mathrm{VP}_5 & 0 & 0 \\ V_{(sa,pc)}P_5 & V_{(s^*a,pc)}P_5 & 0 & V_{(x,x)}P_5 & -V_{(x,y)}P_6 \\ -V_{(sa,pc)}P_6 & -V_{(s^*a,pc)}P_6 & 0 & -V_{(x,y)}P_6 & [V_{(x,x)} + V_{(x,y)}]P_5 \end{bmatrix} \tag{8}$$

$$V_{AC} = \begin{bmatrix} V_{(s,s)}P_1 & 0 & V_{(s,p)}P_2 & -V_{(s,p)}P_1 & 0 \\ 0 & 0 & V_{(s^*,p)}P_2 & -V_{(s^*,p)}P_1 & 0 \\ -V_{(s,p)}P_2 & -V_{(s^*,p)}P_2 & \mathrm{VP}_1 & -V_{(x,y)}P_2 & 0 \\ V_{(s,p)}P_1 & V_{(s^*,p)}P_1 & -V_{(x,y)}P_2 & V_{(x,x)}P_1 & 0 \\ 0 & 0 & 0 & 0 & [V_{(x,x)} - V_{(x,y)}]P_1 \end{bmatrix} \tag{9}$$

$$U_{AC} = \begin{bmatrix} V_{(s,s)}P_3 & 0 & 0 & V_{(s,p)}P_3 & V_{(s,p)}P_4 \\ 0 & 0 & 0 & V_{(s^*,p)}P_3 & V_{(s^*,p)}P_4 \\ 0 & 0 & \mathrm{VP}_3 & 0 & 0 \\ -V_{(s,p)}P_3 & -V_{(s^*,p)}P_3 & 0 & V_{(x,x)}P_3 & V_{(x,y)}P_4 \\ -V_{(s,p)}P_4 & -V_{(s^*,p)}P_4 & 0 & V_{(x,y)}P_4 & [V_{(x,x)} + V_{(x,y)}]P_3 \end{bmatrix} \tag{10}$$

$$U_{CA} = \begin{bmatrix} V_{(s,s)}P_5 & 0 & 0 & -V_{(s,p)}P_5 & V_{(s,p)}P_6 \\ 0 & 0 & 0 & -V_{(s^*,p)}P_5 & V_{(s^*,p)}P_6 \\ 0 & 0 & \mathrm{VP}_5 & 0 & 0 \\ V_{(s,p)}P_5 & V_{(s^*,p)}P_5 & 0 & V_{(x,x)}P_5 & -V_{(x,y)}P_6 \\ -V_{(s,p)}P_6 & -V_{(s^*,p)}P_6 & 0 & -V_{(x,y)}P_6 & [V_{(x,x)} + V_{(x,y)}]P_5 \end{bmatrix} \tag{11}$$

Table 1. Tight-binding parameters (in eV) for bulk BeTe. The off-site matrix elements ($\xi, \xi' = \mathrm{s}, \mathrm{s}^*, \mathrm{p}_x$, and p_y; $\alpha, \alpha' = \mathrm{a}, \mathrm{c}$) are written in the standard notation of Slater–Koster approximation.

$V_{(sa,pc)}$	2.897
$V_{(s^*a,pc)}$	10.871
$V_{(sc,pa)}$	4.686
$V_{(s^*c,pa)}$	4.247
$V_{(s,s)}$	−6.922
$V_{(x,x)}$	0.2147
$V_{(x,y)}$	4.013
E_s^a	−8.857
E_s^c	1.590
$E_{s^*}^a$	61.299
$E_{s^*}^c$	22.736
E_p^a	−0.2297
E_p^c	3.997

where the following notation has been introduced (in the middle columns of the above six matrices) for reasons of space:

$$\mathrm{VP}_1 = [V_{(x,x)} + V_{(x,y)}]P_1$$
$$\mathrm{VP}_3 = [V_{(x,x)} - V_{(x,y)}]P_3$$
$$\mathrm{VP}_5 = [V_{(x,x)} - V_{(x,y)}]P_5$$

and where we have

$$P_1 = \frac{1}{4}[\exp(\mathrm{i}dk_{xy}^-) + \exp(-\mathrm{i}dk_{xy}^+)] \tag{12}$$

$$P_2 = \frac{\sqrt{2}}{4}[\exp(\mathrm{i}dk_{xy}^-) - \exp(-\mathrm{i}dk_{xy}^+)] \tag{13}$$

$$P_3 = \frac{1}{4}\exp(\mathrm{i}dk_{zy}^+) \tag{14}$$

$$P_4 = \frac{\sqrt{2}}{4}\exp(\mathrm{i}dk_{zy}^+) \tag{15}$$

$$P_5 = \frac{1}{4}\exp(\mathrm{i}dk_{zy}^-) \tag{16}$$

$$P_6 = \frac{\sqrt{2}}{4}\exp(\mathrm{i}dk_{zy}^-) \tag{17}$$

with

$$k_{xy}^{\pm} = \sqrt{2}(k_x \pm k_y) \tag{18}$$

$$k_{zy}^{\pm} = \sqrt{2}(k_z \pm k_y) \tag{19}$$

$$d = a_L/4. \tag{20}$$

a_L is the average of the cubic lattice constants of the bulk II–VI compounds and the group IV semiconductor Si or Ge.

The intramaterial matrix elements in the Hamiltonian can be formed uniquely by using the corresponding bulk parameters. For the two intermaterial matrix elements U_{aC} and U_{Ac} at the interface, a simple average of the bulk parameters has been used in the present calculations. The bulk parameters are determined by fitting the first-principles calculation.

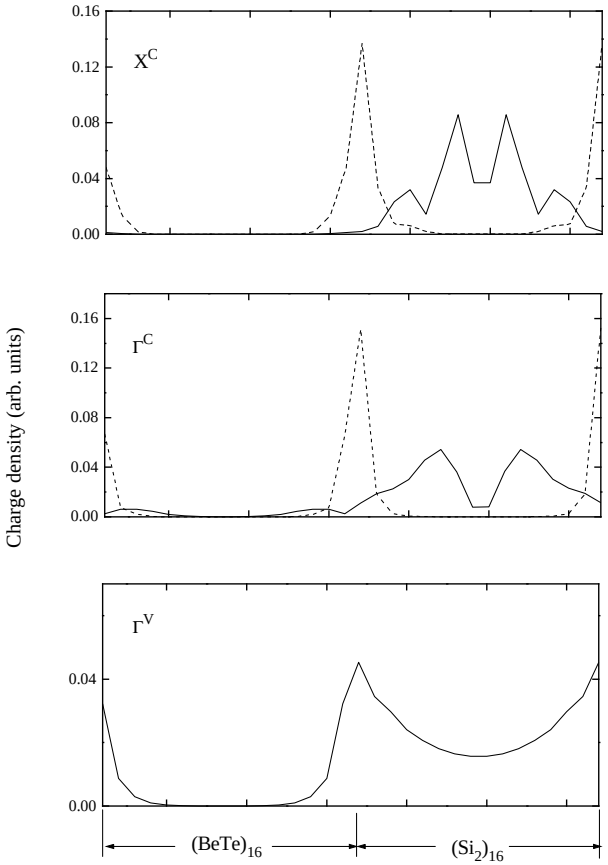

Figure 1. The calculated planar average of the charge densities of the interface (dashed lines) and the confined band-edge (solid lines) states at the Γ and X points for a $(BeTe)_{16}/(Si_2)_{16}$ (110) superlattice with an ideal interface.

Yamaguchi's formulae [16] have been adopted to yield self-consistent results at the X point. These parameters are tested against some well established bulk results [17, 18]. For reference, we give the parameters used in our calculations for bulk BeTe in table 1. Our parameters give the correct indirect gap of 2.95 eV and a correct order of conduction Γ–L–X for bulk BeTe. For the bulk materials Si and Ge we use the parameters given by Vogl *et al* [19]. It should be noted that although only three digits are significant [19], we reproduce the actual numbers used to generate the figures in order to eliminate any problem with round-off errors.

3. Results and discussion

3.1. The localized state at the ideal interface

The planar averages of the charge densities of the X and Γ band-edge states are shown in figure 1 and figure 2 for $(BeTe)_{16}/(Si_2)_{16}$ and $(BeTe)_{16}/(Ge_2)_{16}$ (110) superlattices with ideal interfaces, respectively. At first we assume their valence band offsets ΔE_v to be

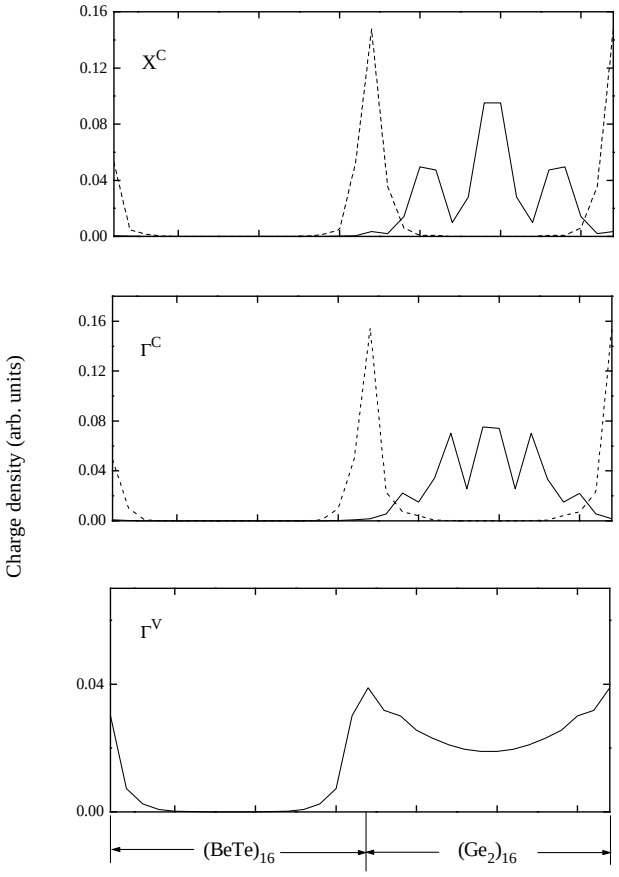

Figure 2. The calculated planar average of the charge densities of the interface (dashed lines) and the confined band-edge (solid lines) states at the Γ and X points for a $(BeTe)_{16}/(Ge_2)_{16}$ (110) superlattice with an ideal interface.

1.03 eV (BeTe/Si) and 1.31 eV (BeTe/Ge) as given by Harrison's theory [20]. Two clearly localized interface state bands, well separated from each other, are found at the interfaces of the BeTe/Si and BeTe/Ge systems, where the Be–Si and Te–Si bonds in the BeTe/Si system appear equivalently to the Be–Ge and Te–Ge bonds in the BeTe/Ge system. The interface states appear over an extended region of $\boldsymbol{k}$-space. Their relative positions are changed by varying ΔE_v, but they do not disappear from the gap for all possible valence band offsets based on the band-structure calculations in the full Brillouin zone. We find that parts of the interface band with higher energy are pushed into the conduction bands, in agreement with the experimental consensus [21].

In addition, from figure 1 and figure 2, one can see that all of the band-edge states are confined in the two dimensions—silicon or germanium wells respectively. We suggest that this is due to the large band gap of BeTe which causes strong quantum confinement in the small-gap layers—Si or Ge quantum wells. Therefore, it is reasonable to believe that these states originate from those of group IV semiconductors via the zone-folding effects.

In order to check the influence of the interfacial chemistry, a pseudobinary semiconductor alloy, $Si_{1-x}Ge_{1+x}$, is used to allow there to be a continuous range of materials

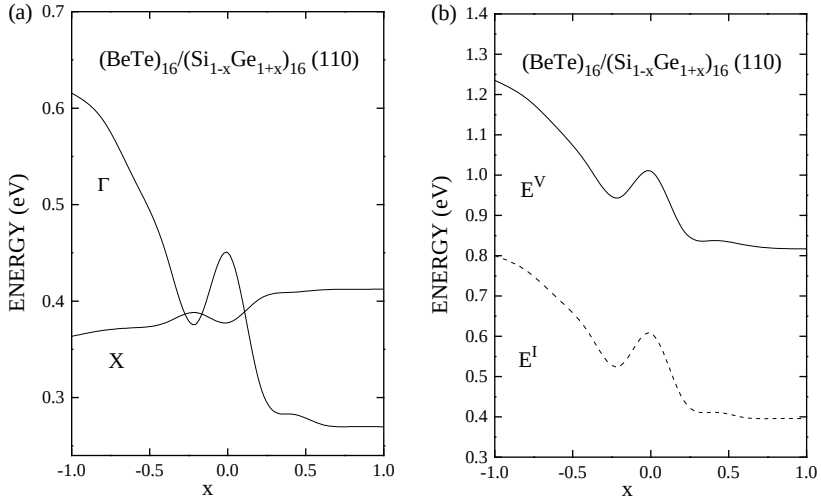

Figure 3. (a) The difference between the interface states and the confined conduction band-edge states of the pseudobinary semiconductor alloy $Si_{1-x}Ge_{1+x}$ at some high-symmetry points, where $\Gamma = \Gamma^C - \Gamma^I$ and $X = X^C - X^I$. (b) The fundamental energy gap and interface state, shown as a solid line and a dashed line respectively, for a $(BeTe)_{16}/(Si_{1-x}Ge_{1+x})_{16}$ (110) superlattice with an ideal interface.

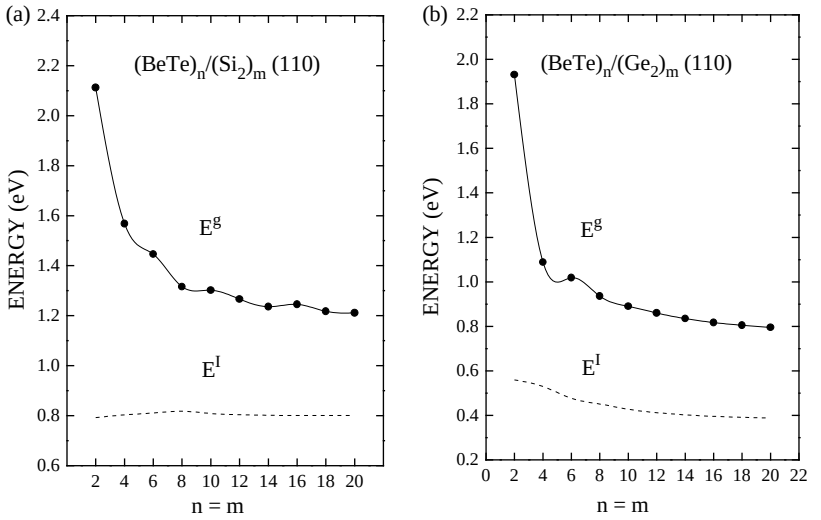

Figure 4. The band gaps E_g of $(BeTe)_n/(Si_2)_m$ (a) and $(BeTe)_n/(Ge_2)_m$ (b) (110) superlattices as functions of the number of layers $n = m$. The relative positions of the interface band E^I are also drawn. The zero of the energy is the valence band maximum of the superlattice.

parameters, tunable by changing the composition x. The tight-binding parameters for bulk SiGe alloy can be written as

$$E(A_{1-x}B_{1+x}) = ((1-x)E(A) + (1+x)E(B))/2. \tag{21}$$

Figure 3(a) shows the differences between the interface state and the confined conduction band-edge state at some high-symmetry points obtained by continuously changing the

composition x, where $\Gamma = \Gamma^C - \Gamma^I$ and $\mathrm{X} = \mathrm{X}^C - \mathrm{X}^I$. The fundamental energy gap versus the composition x is plotted in figure 3(b) as a solid line, and the interface state is also drawn in the figure as a dashed line. For a fixed BeTe layer with $n = 16$, the interface state and the energy gap reach their local maxima concurrently as $x = 0$. The tendencies of the energy gap and the interface state position with variation of the composition x are quite similar.

3.2. Band structure

The fundamental band gaps of the $(\mathrm{BeTe})_n/(\mathrm{Si}_2)_m$ and $(\mathrm{BeTe})_n/(\mathrm{Ge}_2)_m$ (110) superlattices with ideal interfaces are given as functions of $n = m$ in figures 4(a) and 4(b) respectively. The interface states E^I are plotted—dashed lines in figure 4—for both systems, where the zero of energy corresponds to the top of the valence band. It is found that the lowest transition is the indirect Γ-to-$\tilde{\mathrm{X}}$ one for all BeTe/Si superlattices, where $\tilde{\mathrm{X}}$ is near to the X point. For the BeTe/Ge system, it is the Γ-to-M ($n = m > 10$) and Γ-to-$\tilde{\mathrm{X}}$ ones ($n = m \leqslant 10$).

The quantum confinement is most dramatic, as illuminated in figure 4, as the band gap rises sharply on decreasing the superlattice period. However, it is found that the fundamental band gaps of the $(\mathrm{BeTe})_n/(\mathrm{Si}_2)_m$ or $(\mathrm{BeTe})_n/(\mathrm{Ge}_2)_m$ (110) superlattices do not change significantly, as expected, on varying the BeTe layer thickness for a fixed number of Si or Ge layers. It is concluded that the Si or Ge layer thickness is crucial in determining the fundamental gap of the BeTe/Si or BeTe/Ge superlattice.

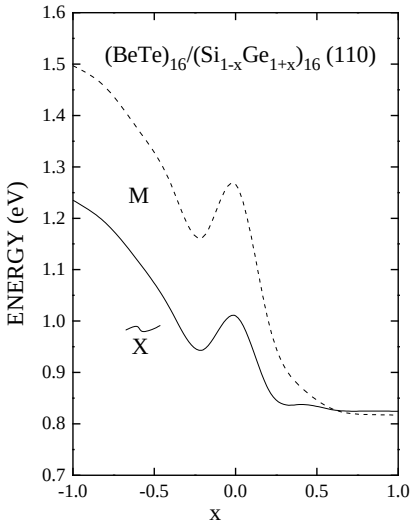

Figure 5. Energies at some high-symmetry points at the $\tilde{\mathrm{X}}$ point (solid line) and the M point (dashed line) for a $(\mathrm{BeTe})_{16}/(\mathrm{Si}_{1-x}\mathrm{Ge}_{1+x})_{16}$ (110) superlattice with an ideal interface. The lowest transitions are the Γ-to-M ($x < 0.61$) and Γ-to-$\tilde{\mathrm{X}}$ ($x > 0.61$) ones.

Furthermore, figure 5 shows how the relative positions of the two minima of the valence band at the $\tilde{\mathrm{X}}$ point (solid line) and M point (dashed line) change on varying the composition x for the $(\mathrm{BeTe})_{16}/(\mathrm{Si}_{1-x}\mathrm{Ge}_{1+x})_{16}$ (110) superlattice, where the zero of energy corresponds to the top of the valence band. From figure 5, one can see that the conductance band minima of the $(\mathrm{BeTe})_{16}/(\mathrm{Si}_{1-x}\mathrm{Ge}_{1+x})_{16}$ (110) superlattice are located at the $\tilde{\mathrm{X}}$ point while

the composition x is less than 0.61. However, as more germanium atoms are added into the pseudobinary semiconductor alloy SiGe layer, the conductance band-edge energy at the M point decreases more rapidly than that of the $\tilde{X}$ point does, and when the composition x is greater than 0.61, the conductance band minima are located at the M point. In other words, the symmetry of the conductance band changes at around $x = 0.61$.

4. Conclusion

A detailed investigation of the interfacial chemistry, electronic structure, and optical transition in the $(\text{II–VI})_n/(\text{IV}_2)_m$ (110) superlattice has been performed for a wide range of $n, m \leqslant 20$ by using a semiempirical tight-binding method. Two empty interface bands are identified in the upper region of the gap in the superlattice systems, which extend over a quite different region of $\boldsymbol{k}$-space. It is found the SiGe layer plays a dominant role in determining the fundamental gap of the superlattice system due to the strong quantum confinement effect. For valence band discontinuities of $\Delta E_v = 1.03$ eV for the BeTe/Si superlattice and $\Delta E_v = 1.31$ eV for the BeTe/Ge superlattice, as given by Harrison's theory, the band gap between the confined band-edge states increases sharply (up to 2.11 eV for BeTe/Si and 1.93 eV for BeTe/Ge at the $\tilde{X}$ point for $n = m = 2$) on the superlattice period being decreased. By checking the electronic structure of $\text{BeTe/Si}_{1-x}\text{Ge}_{1+x}$ with the composition x changing from -1 to 1, we found that the electronic and interfacial properties are different to those of II–VI compounds grown on pure group IV semiconductors, but fairly close to their average in all cases. Our calculation shows that behaviour of the interface states of these calculated systems appears to undergo no major change within the range of composition x examined. The results presented in this work should establish an understanding of the fundamental electronic properties of the superlattices fabricated from II–VI and group IV semiconductors.

Acknowledgment

This work was partly supported by Chinese NSF Grant No 69525409.

References

[1] Pérez-Díaz J L and Muñoz M C 1996 *Phys. Rev. Lett.* **76** 4967
[2] Salib M S, Nickel H A, Herold G S, Prtrou A, McCombe B D, Chen R, Bajaj K K and Schaff W 1996 *Phys. Rev. Lett.* **77** 1135
[3] Messica A, Soibel A, Meirav U, Stern A, Shtrikman H, Umansky V and Mahalu D 1997 *Phys. Rev. Lett.* **78** 705
[4] Osbourn G C 1982 *J. Appl. Phys.* **53** 1586
[5] Pearsall T P, Pollak F H, Bean J C and Hull R 1986 *Phys. Rev.* B **133** 6281
[6] Bean J C 1985 *Science* **230** 127
[7] Pearsall T P, Beark F, Feldman L C, Bonar J M, Mannaerts J P and Ourmazd A 1987 *Phys. Rev. Lett.* **58** 729
[8] Miller R C, Kleinman D A and Savage A 1963 *Phys. Rev. Lett.* **11** 146
[9] Scholl F W and Tang C L 1973 *Phys. Rev.* B **8** 4607
[10] Fisher A J, Kim D S, Hays J, Sham W, Song J J, Eason D B, Ren J, Schetzina J F, Luo H, Furdyna J K, Zhu Z Q, Yao T, Klem J F and Shafer W 1994 *Phys. Rev. Lett.* **73** 2378
[11] Romano L T, Bringans R D, Knall J, Biegelsen D K, Garcia A and Northrup J E 1994 *Phys. Rev.* B **50** 4416
[12] Zhou X C and Kirk W P 1994 *Mater. Res. Soc. Symp. Proc.* **318** 307
[13] Zhou X C, Spencer G F, Li F and Kirk W P 1995 *AIP Proc.* **325** 227
[14] Wang E G and Ting C S 1995 *Phys. Rev.* B **51** 9791

[15] Wang E G 1996 *Appl. Surf. Sci.* **104** 626
[16] Yamaguchi E 1988 *J. Phys. Soc. Japan* **57** 2461
[17] Stukel D J 1970 *Phys. Rev.* B **2** 1852
[18] Sarkar R L and Chatterjee S 1977 *J. Phys. C: Solid State Phys.* **10** 47
[19] Vogl P, Hjalmarson H P and Dow J D 1983 *J. Phys. Chem. Solids* **44** 365
[20] Harrison W A 1980 *Electronic Structure and the Properties of Solids* (San Francisco, CA: Freeman)
[21] Milnes A G and Feucht D L 1972 *Heterojunctions and Metal–Semiconductor Junctions* (New York: Academic)